Title

Low-temperature growth of single-crystal $Cu(In,Ga)Se_2$ films by Pulsed Electron Deposition technique

Author names

S. Rampino[1], M. Bronzoni[1], L. Colace[2], P. Frigeri[1], E. Gombia[1], C. Maragliano[3], F. Mezzadri[1], L. Nasi[1], L. Seravalli[1], F. Pattini[1], G. Trevisi[1], M. Motapothula[4], T. Venkatesan[4] and E. Gilioli[1]

Affiliation

[1] IMEM-CNR Institute, Parco Area delle Scienze 37/A, 43124 Parma, Italy

[2] Department of Engineering - University "Roma Tre", Via Vito Volterra, 62 - 00146 Rome Italy

[3] LENS Laboratory, Masdar Institute of Science and Technology, Masdar City, PO Box 54224, Abu Dhabi, United Arab Emirates

[4] NUSNNI-NanoCore, National University of Singapore, Singapore 117576, Singapore

Corresponding author e-mail address: rampino@imem.cnr.it

Abstract

High quality epitaxial crystalline $Cu(In,Ga)Se_2$ (CIGS) films were grown on n-type (100) - Germanium (Ge) substrates using Pulsed Electron Deposition (PED) technique at a remarkably low substrate temperature of 300 °C, thanks to the high-energy of adatoms arriving to the substrate. The crystalline quality was confirmed by X-Ray Diffraction techniques and from Transmission Electron Microscopy and the only defects found were

twin boundaries along the (112) direction in these CIGS films; surprisingly neither misfit dislocations nor Kinkerdall voids were observed. A 100 meV optical band located below the band edge was observed by Photoluminescence technique. Current-Voltage and Capacitance-Voltage measurements confirm an intrinsic p-type conductivity of CIGS films, with a free carrier concentration of ≈3.5x10^{16} cm^{-3}. These characteristics of crystalline CIGS films are crucial for a variety of potential applications, such as more efficient absorber layers in single-junction and as an integral component of multi-junction thin-film solar cells.

1. INTRODUCTION

Thin film solar cells based on polycrystalline Cu(In,Ga)Se_2 (CIGS) are considered to be among the most promising photovoltaic devices due to their high energy harvesting efficiency, long term stability and industrial scalability. Recent developments include record lab-scale cells with conversion efficiency above 20% on both rigid [1] and flexible substrates [2].

Even though the performance of CIGS devices is approaching the crystalline Silicon solar cell efficiency, the best lab results are still quite far from the Shockley-Queisser theoretical limit of 33% [3]. Despite extensive work carried out on the loss mechanisms in CIGS solar cells to achieve the theoretically predicted limit, this topic is still under intense debate. The most relevant losses are related to the following effects [4,5]: i) Shockley-Read-Hall recombination in the space charge region and at the grain boundaries, ii) bandgap fluctuations induced by lateral stoichiometry non-uniformity, iii) low electron mobility due to impurity scattering and band bending at charged grain boundaries and iv) fluctuations of the electrostatic potential caused by extended defects such as dislocations and grain boundaries.

Although the beneficial role of grain boundaries as hole barriers in polycrystalline films is widely accepted, their presence induces strong fluctuations on the electrostatic potential, leading to an increase of the diode saturation current and to the consequent net reduction of the open circuit voltage [4,5]. From these considerations, the enhancement of the crystal quality is a crucial requirement for reducing efficiency losses in CIGS solar cells.

Aiming to investigate the role of the CIGS crystal structure and grain size on the solar cell performance, in previous studies we have developed a three-dimensional model for ZnO/CdS/CIGS/Mo solar cells to be included in Sentaurus Technology Computer Aided Design (TCAD) semiconductor device simulation tool [6]; the simulations strongly indicated that the cell efficiency would benefit from larger grain size over a wide range of values of the photogenerated carrier's surface recombination rate, both at the CdS/CIGS heterojunction (S_n), and at the grain boundaries (V_r), as summarized in Figure 1.

The results suggest that significantly improved solar cell absorbers can be expected from single crystal CIGS films, obtainable only by epitaxial growth on substrates with reduced lattice mismatch. GaAs has been exploited as epitaxial substrate in previous works [7-9]: from these studies, it turned out that substrate temperatures above 550°C were found necessary for the epitaxial growth of CIGS by Molecular Beam Epitaxy (MBE) and Metal Organic Chemical Vapour Deposition (MOCVD) techniques [10].

In this paper we report on the epitaxial deposition of CIGS films on Germanium wafers at low substrate temperature (300°C) by the Pulsed Electron Deposition (PED) technique. Germanium was chosen as epitaxial substrate alternative to GaAs, because of: i) its lattice parameter (a = 5.652 Å) that yields a lattice mismatch <1%, ii) its similar thermal expansion coefficient (5.8×10^{-6} K^{-1}), and, contrary to GaAs, iii) its capability to act as low-bandgap absorber in a hypothetical CIGS/Ge-based tandem solar device. PED technique was proven to be a viable route for depositing high-quality CIGS: we have

recently reported 15%-efficient CIGS-based solar cells fabricated by PED on Mo-coated glass substrates at 270°C [11]. We emphasize that the above mentioned TCAD simulations are in good agreement with the experimentally measured photovoltaic parameters, the efficiency value expected being ≈15% (average grain size ≈1μm and S_n and V_r ≈10^5 cm/s). The remarkably low deposition temperature is a characteristic of the PED technique, where a high-energy evaporation plume (from few to thousands of eV), enhances the surface mobility of the adatoms arriving at the substrate regardless of the substrate temperature [12]. We conclude that the deposition of high-quality epitaxial CIGS films by PED can be therefore carried out at a notably lower substrate temperature compared to MBE and MOCVD.

2. EXPERIMENTAL

CIGS films have been grown using a commercial PED system (Neocera Inc.); the operation principles of the PED process and the CIGS growth conditions are reported elsewhere [13].

As a substrate, n-type Ge wafer (100) (n=1x$10^{17}$$cm^{-3}$, 15x15 mm^2 wide) with a 6° miscut towards [110] has been used, treated in diluted hydrofluoric acid for removing the surface oxides. The substrates were placed 8 cm away from the target, under a graphite susceptor heated by halogen lamps and its temperature was kept at 300 °C and monitored by a thermocouple. Analogously to the solar cells deposited on Mo-coated glass by PED, the thickness of CIGS films was ≈1.6 μm.

The structural properties of the samples were characterized by X-ray diffraction (XRD), with a Siemens D500 system equipped with a Cu Kα X-ray source (λ = 1.5406 Å) in the Bragg-Brentano geometry. Transmission Electron Microscopy (TEM) was carried out on sample cross-sections using a JEOL-2200FS microscope working at 200keV for evaluating the film thickness and the epitaxial quality of CIGS near the interface with Ge.

TEM specimens were prepared by mechanical grinding followed by Ar ion milling. The film composition was conducted in spot mode by means of an Energy Dispersive X-Ray Spectroscopy (EDS) detector mounted on the TEM system. CIGS films were optically characterized by Photoluminescence (PL) technique performed at 10K, using a 100 mW, 532 nm Solid State laser. The emitted light was detected in the 0.8÷2.0 eV range by a Fast-Fourier Transform spectrometer and a cooled Ge detector.

The current-voltage (I-V) characteristics of the CIGS/Ge diodes were measured by a Keithley 236 source-measure unit. The net carrier density in the CIGS layer was estimated from the capacitance-voltage (C-V) characterization of the CIGS/Ge heterojunction at 300K by using an AC test signal with 25 mV amplitude at a frequency of 1 MHz. For the CIGS/Ge heterojunction measurements, ohmic contacts were thermally evaporated both on CIGS (860 μm-diameter Au dots) and on n-type Ge (AuCr stripes). Our standard solar cells with polycrystalline Na-free CIGS absorber in the structure: ZnO:Al/CdS/CIGS/Mo, were used to compare the free carrier concentration in polycrystalline and epitaxial CIGS layers.

3. RESULTS AND DISCUSSION

3.1 *Crystal structure and chemical composition*

The XRD patterns of CIGS films grown on Ge at 300°C in comparison with a typical polycrystalline CIGS deposited on Mo/Glass under the same conditions are shown in Figure 2. While the polycrystalline CIGS/Mo/Glass pattern exhibits the expected preferred grain orientation along the (112) direction [13], only the (008)-CIGS and the (400)-Ge reflections are observed in the case of CIGS/Ge, thus confirming epitaxial growth of CIGS on (100)-Ge. By analyzing the position of the (008)-CIGS peak, a lattice parameter c = 11.383 Å of the CIGS tetragonal phase can be calculated. The achievement of the

epitaxial growth of CIGS on Ge at such low temperature is a noteworthy result when compared with previous studies where substrate temperatures larger than 550°C were found necessary for epitaxially growing CIS and CIGS films by traditional deposition techniques as MBE and Sputtering[14,15].

High Resolution Transmission Electron Microscopy (HRTEM) analysis confirms the epitaxial growth at the CIGS/Ge interfaces (Figure 3). The corresponding Fast Fourier Transform (FFT) image shown in the inset reveals the presence of a perfect epitaxial relationship CIGS(001)//Ge(001), with a lattice mismatch within the instrument sensitivity (~1%). Neither dislocations nor Kinkerdall voids, commonly noticed in CIGS/GaAs systems [8,10,16], are observed.

The High-Angle Annular Dark-Field (HAADF) cross-sectional image of the sample reported in Figure 4 confirms that the single crystal structure is preserved over the whole CIGS thickness. Twin boundaries along the (112) direction start to appear at ~300 nm from the CIGS/Ge interface: these defects have been noticed also in Cu(In,Ga)S_2/Si heterostructures, and their origin seems to be related to the relaxation of lattice strain accumulated during the growth process [17].

EDS measurements reveal a strong Ga and Cu gradients along the CIGS thickness, with Ga/(In+Ga) (GGI) and Cu/(In+Ga) (CGI) ratios starting from 0.54 and 1.13 at the interface, respectively, and decreasing to 0.30 and 0.85 near the CIGS surface (Figure 5). This Ga enrichment at the interface has been already observed by other authors at the epi-CIGS/GaAs interface and it was explained in terms of Ga out-diffusion from GaAs [4,8]. Ga contamination from the substrate is clearly ruled out in our case. Since in CIGS/Mo/Glass samples, neither GGI (=0.30) nor CGI (=0.85) undergo a variation along the whole CIGS thickness, it can be inferred that in CIGS/Ge system the chemical composition of the layer is self-adapted in order to minimize the lattice mismatch with the substrate. Indeed, for GGI = 0.54, the corresponding calculated lattice mismatch with Ge

becomes <0.5% [8]. This effect could explain why misfit dislocations were not detected at the heterostructure interface.

3.2 *Optical properties*

Photoluminescence spectra of CIGS/Ge taken at 10K exhibit a dominant narrow symmetric peak centered around 100 meV below the band edge = 1.17 eV (Figure 6), calculated on the basis of the GGI ratio value at the surface = 0.30 [18]. The average FWHM value of the peak is ≈55 meV. This emission is usually ascribed to a donor-acceptor pair (DAP) emission related to V_{Cu} and V_{Se} levels [19]. This PL spectrum is very similar to that measured on $CuInSe_2$ epitaxial films grown at 660°C on (100)-GaAs wafers [20].

On the other hand the PL spectrum of CIGS/Ge appears slightly different from that of polycrystalline CIGS/Mo/Glass grown at the same substrate temperature, where two distinct emission peaks are visible. While the peak at higher energy can be associated with the same DAP $V_{Se} \rightarrow V_{Cu}$ transition of CIGS/Ge, the latter is usually attributed to the $In_{Cu} \rightarrow V_{Cu}$ transition [19]. The absence of a radiative recombination due to the In_{Cu} antisite in CIGS/Ge confirms a lower density of cation substitutional defects in epitaxial CIGS with respect to polycrystalline layers. Other relevant differences between epitaxial and polycrystalline CIGS concern: i) the intensity of the PL emission, stronger by a factor of 7 in CIGS/Ge, and ii) the spatial uniformity of the spectra: while in polycrystalline CIGS the relative weight of the two peaks changes considerably along the sample area, the shape of the PL spectrum of the CIGS/Ge is unchanged over different regions of the sample. This latter confirms a higher compositional and structural uniformity of the epitaxial CIGS material in comparison with the polycrystalline one.

3.3 Electrical properties

Figure 7 shows the current-voltage characteristics of the CIGS/Ge heterostructure at 300K. The good rectifying properties of the device confirm the intrinsic p-type conduction in CIGS layer, forming a good heterojunction with the n-type Ge substrate. The sample shows a high spatial uniformity, since similar I-V characteristics have been obtained over different regions. The calculated diode ideality factor is ~1.98.

The space charge density profiles calculated from C-V curves at 300K of epi-CIGS/Ge diodes and ZnO:Al/CdS/poly-CIGS/Mo solar cells are compared in Figure 8. Following a commonly accepted approach to interpret C-V spectra in CIGS-based devices [21,22], the minimum in space charge density profile has been taken as a value of free hole concentration, resulting in $p= 3.5x10^{16}$ cm^{-3} in the case of epitaxial CIGS, about two orders of magnitude larger than in polycrystalline CIGS solar cell ($p= 3.9x10^{14}$ cm^{-3}). This large difference can be accounted for by different degrees of electrical compensation in the two systems. While compensation is a well-known feature of Na-free polycrystalline CIGS [23], where a high density of both donor and acceptor defects are simultaneously present, this effect seems to be less prominent in single-crystal CIGS. Since In_{Cu} antisites are known to be the main compensating donors in CIGS, it can be concluded that the density of such substitutional defects in epitaxial CIGS is lower than in poly-CIGS. This hypothesis is in agreement with the observed annihilation of the emission peak related to $In_{Cu} \rightarrow V_{Cu}$ in the PL spectra of CIGS/Ge samples.

4. CONCLUSIONS

1.6μm-thick single-crystal CIGS films have been successfully grown on Ge by PED technique. The unusual high-energy process provided by the PED technique, enables the CIGS epitaxial growth at much lower temperatures (300°C) with respect to traditional MBE or MOCVD techniques (>550°C). No linear defects, as misfit dislocation, were detected at

the CIGS/Ge interface; twin boundaries along the (112) direction are the only crystalline defects revealed in the epilayer. The chemical composition of CIGS/Ge films is not uniform along the film thickness, in contrast with the observed constant trend in polycrystalline CIGS films grown on Mo-coated glass under the same conditions. This gradient, likely to occur in the epitaxial films to minimize the lattice mismatch with Ge substrate, is comparable to the intentional distribution obtained in high-efficiency poly-crystalline CIGS solar cells [2].

The improved crystal quality enhances the optical and electrical properties in the CIGS/Ge films with respect to the CIGS/Mo/Glass reference sample. A possible reduction of the number of substitutional In_{Cu} defects in single crystal CIGS could be the main reason for both the quenching of the low-energy peak in PL spectrum and the reduction of the electrical compensation of epitaxial CIGS as compared to the polycrystalline layers. As suggested by the simulations, these features of single-crystal CIGS promise better performances as absorber layers in single and multi-junction thin-film solar cells. Contrary to CIGS/GaAs, CIGS/Ge epitaxial system could be also used for fabricating a new-generation of multi-junction solar cells, based on the combination of a bottom Ge homojunction and top epi-CIGS/CdS heterojunction; the fabrication of epi-CIGS/CdS solar cells on p^+-type Ge wafer is in progress.

Finally, we have demonstrated that PED technique is an accessible ~~and cost-effective~~ deposition route not only to deposit efficient polycrystalline CIGS-based solar cells, but also to grow materials with superior crystal quality. Besides opening up interesting opportunities in the study of the controversial correlation between structural/compositional defects and performance of thin film photovoltaic devices, the inherent scalability of the PED process portends a possible route to the manufacture of large scale, high quality crystalline CIGS based PV films in the near future.

ACKNOWLEDGEMENTS

The authors acknowledge Dr. D. Calestani (IMEM-CNR) for CIGS target synthesis, Dr. M. Calicchio (IMEM-CNR) for electrical measurements, Mr. T. Besagni and Mrs. P. Ferro (IMEM-CNR) for XRD analysis. The authors are grateful to Dr. M. Bosi, Dr. F. Bissoli, Dr. M. Mazzer and Dr. N. Marigo (IMEM-CNR) for fruitful discussion. This work has been partially supported by the Italian Ministry of University and Research (FIRB-2008 Project, Code RBFR08P44S_003: "*Nanostructured and Thin-Films Photovoltaic Devices for spectral splitting concentration systems*") and by CNR (Programme "*Progetto Bandiera - La Fabbrica del Futuro", project "MaCISte, "Mature CIS-based solar cells technology*"). T. Venkatesan would like to acknowledge support from the SINBERISE project of the National Research Foundation.

REFERENCES

[1] P. Jackson, D. Hariskos, R. Wuerz, W. Wischmann, M. Powalla, Compositional investigation of potassium doped Cu(In,Ga)Se_2 solar cells with efficiencies up to 20.8%, Phys. Status Solidi RRL 8 (2014) 219-222.

[2] A. Chirilă, P. Reinhard, F. Pianezzi, P. Bloesch, A. R. Uhl, C. Fella, L. Kranz, D. Keller, C. Gretener, H. Hagendorfer, D. Jaeger, R. Erni, S. Nishiwaki, S. Buecheler, A. N. Tiwari, Potassium-induced surface modification of Cu(In,Ga)Se_2 thin films for high-efficiency solar cells, Nat. Mat. 12 (2013) 1107-1111.

[3] W. Shockley, H.J. Queisser, Detailed Balance Limit of Efficiency of p-n junction Solar Cells, J. Appl. Phys. 32 (1962) 510-519.

[4] S. Siebentritt, What limits the efficiency of chalcopyrite solar cells?, Sol. Energy Mater. Sol. Cells 95 (2011) 1471-1476.

[5] J. H. Werner, J. Mattheis, U. Rau, Efficiency limitations of polycrystalline thin film solar cells: case of Cu(In,Ga)Se_2, Thin Solid Films 480–481 (2005) 399-409.

[6] C. Maragliano, L. Colace, M. Chiesa, S. Rampino, M. Stefancich, Three-Dimensional Cu(InGa)Se_2 Photovoltaic Cells Simulations: Optimization for Limited-Range Wavelength Applications, IEEE J. Photovoltaics 3 (2013) 1106-1112.

[7] S. Niki, Y. Makita, A. Yamada, O. Hellman, P.J. Fons, A. Obara, Y. Okada, R. Shioda, H. Oyanagi, T. Kurafuji, S. Chichibu, H. Nakanishi, Heteroepitaxy and characterization of $CuInSe_2$ on GaAs(001), J. Cryst. Growth 150 (1995) 1201-1205.

[8] D. Liao, A. Rockett, Epitaxial growth of Cu(In,Ga)Se_2 on GaAs(110), J. Appl. Phys., 91 (2002) 1978-1983.

[9] L. Roussak, G. Wagner, L. Makhova, I. Konovalov, Epitaxial $CuIn_{1-x}Ga_xSe_2$/ZnS heterostructures grown on (001)GaAs by co-evaporation, Phys. Status Solidi C 6, (2009) 1287-1290.

[10] C. H. Lei, A. A. Rockett, I. M. Robertson, N. Papathanasiou, S. Siebentritt, Interface reactions and Kirkendall voids in metal organic vapor-phase epitaxy grown Cu(In,Ga)Se_2 thin films on GaAs, J. Appl. Phys. 100 (2006) 114915.

[11] S. Rampino, N. Armani, F. Bissoli, M. Bronzoni, D. Calestani, M. Calicchio, N. Delmonte, E. Gilioli, E. Gombia, R. Mosca, L. Nasi, F. Pattini, A. Zappettini, M. Mazzer, 15% efficient Cu(In,Ga)Se_2 solar cells obtained by low-temperature pulsed electron deposition, Appl. Phys. Lett. 101 (2012) 132107.

[12] M. D. Strikovski, J. Kim, S. H. Kolagani, Plasma Energetics in Pulsed Laser and Pulsed Electron Deposition, in: Handbook of Crystal Growth, ed. Springer, Berlin Heidelberg, 2010, ch. 35, pp. 1200-1201.

[13] S. Rampino, F. Bissoli, E. Gilioli, F. Pattini, Growth of Cu(In,Ga)Se_2 thin films by a novel single-stage route based on pulsed electron deposition, Prog. Photovolt.: Res. Appl. 21 (2013) 588-594.

[14] B. Schumann, A. Tempel, G. Kühn, Epitaxial layers of $CuInSe_2$, Sol. Cell 16 (1986) 43-63.

[15] B. J. Stanbery, S. Kincal, S. Kim, C. H. Chang, S. P. Ahrenkiel, G. Lippold, H. Neumann, T. J. Anderson, O. D. Crisalle, Epitaxial growth and characterization of $CuInSe_2$ crystallographic polytypes, J. Appl. Phys. 91 (2002) 3598-3604.

[16] L.-C. Yang, Sputtered epitaxial chalcopyrite CuInSe2 films grown on GaAs substrates, J. Crys. Growth 294 (2006) 202-208.

[17] J. Cieslak, T. Hahn, J. Kräußlich, H. Metzner, J. Eberhardt, W. Witthuhn, Twinning in Cu(In,Ga)S_2, Phys. Status Solidi C 6 (2009) 1023-1026.

[18] R. Chakrabarti, B. Maiti, S. Chaudhuri, A.K. Pal, Photoconductivity of Cu(In, Ga)Se_2 films, Sol. En. Mat. Sol. Cells 43 (1996) 237-247.

[19] S. Zott, K. Leo, M. Ruck, H. W. Schock, Radiative recombination in $CuInSe_2$ thin films, J .Appl. Phys. 82 (1997) 356-367.

[20] D. N. Hebert, J. A. N. T. Soares, A. A. Rockett, Photoluminescence and Photoluminescence Excitation Spectroscopy of Cu(In,Ga)Se_2 Thin Films, Mater. Res. Soc. Symp. Proc. 1165 (2010) 93-100.

[21] M. Cwil, M. Igalson, P. Zabierowski, S. Siebentritt, Charge and doping distributions by capacitance profiling in Cu(In,Ga)Se_2 solar cells, J. Appl. Phys. 103 (2008) 063701.

[22] P. Salomé, V. Fjallstrom, A. Hultqvist, P. Szaniawski, U. Zimmermann, M. Edoff, The effect of Mo back contact ageing on Cu(In,Ga)Se_2 thin-film solar cells, Prog. Photovolt: Res. Appl. 22 (2014) 83–89.

[23] A. Rockett, The effect of Na in polycrystalline and epitaxial single-crystal $CuIn_{1-x}Ga_xSe_2$, Thin Solid Films 480–481 (2005) 2–7.

LIST OF FIGURES

Figure 1 - Conversion efficiency versus grain size for different surface recombination rates at the CdS/CIGS heterojunction (S_n). The efficiency trends are simulated for two different recombination velocities at the grain boundaries, $V_r=10^5$cm/s (top) and $V_r=10^7$cm/s (bottom).

Figure 2 – XRD patterns of an epitaxial CIGS/Ge heterostructure (blue line) and a typical polycrystalline CIGS/Mo/Glass (red line) grown at the same temperature = 300°C. The inset shows a close-up of the CIGS/Ge diffraction pattern.

Figure 3 - HRTEM image of the CIGS/Ge interface. The insets show the corresponding FFT patterns.

Figure 4 - HAADF cross-sectional image of the CIGS/Ge structure. The inset shows a HRTEM image of the twin boundaries along the (112) direction.

Figure 5 - Distribution of GGI and CGI ratios along the CIGS thickness in both epitaxial and polycrystalline films. The dashed lines indicate the values of the two ratios in the starting CIGS target.

Figure 6 - Representative PL spectra of CIGS/Ge (up) and CIGS/Mo/glass (down) samples, grown at the same substrate temperature =300°C. The spectra were taken at 10K.

Figure 7 – Forward (triangles) and reverse (circles) bias current-voltage characteristics of the CIGS/Ge heterostructures.

Figure 8 – Space charge density profiles in both epitaxial (blue dots) and polycrystalline (red diamonds) CIGS layers calculated from CV measurements at 300K.

Figure 1

Click here to download high resolution image

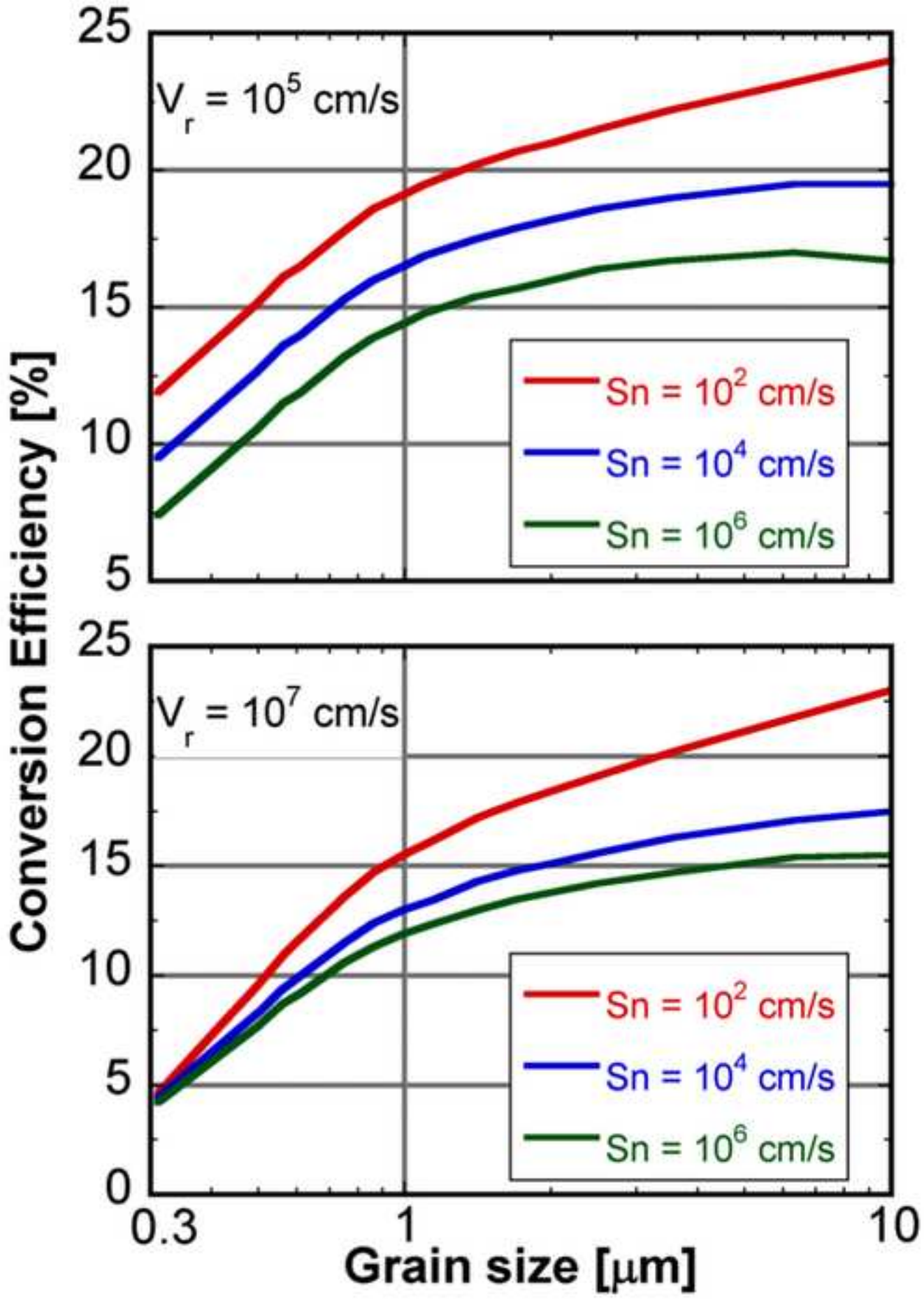

Figure 2
Click here to download high resolution image

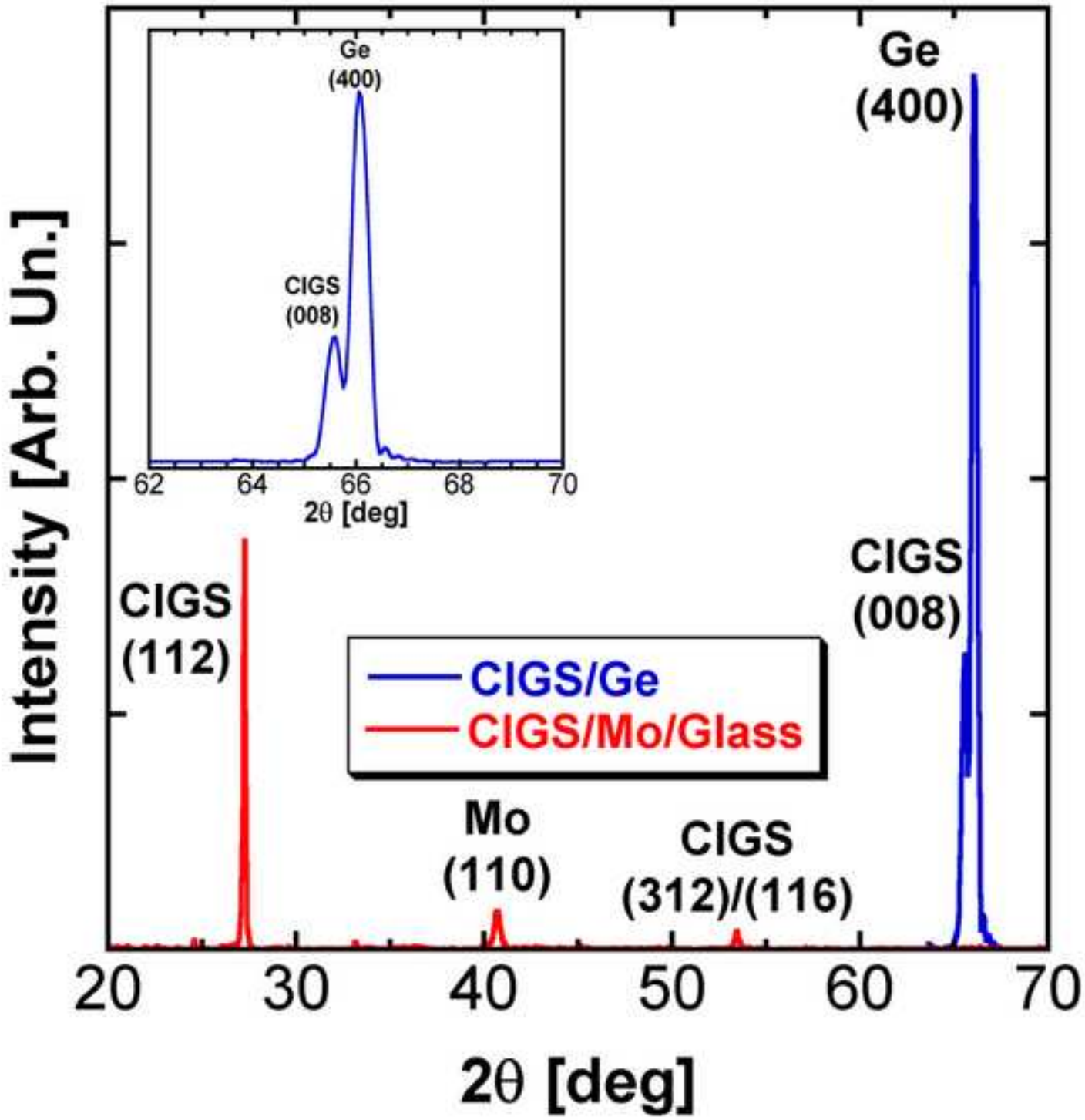

Figure 3

Click here to download high resolution image

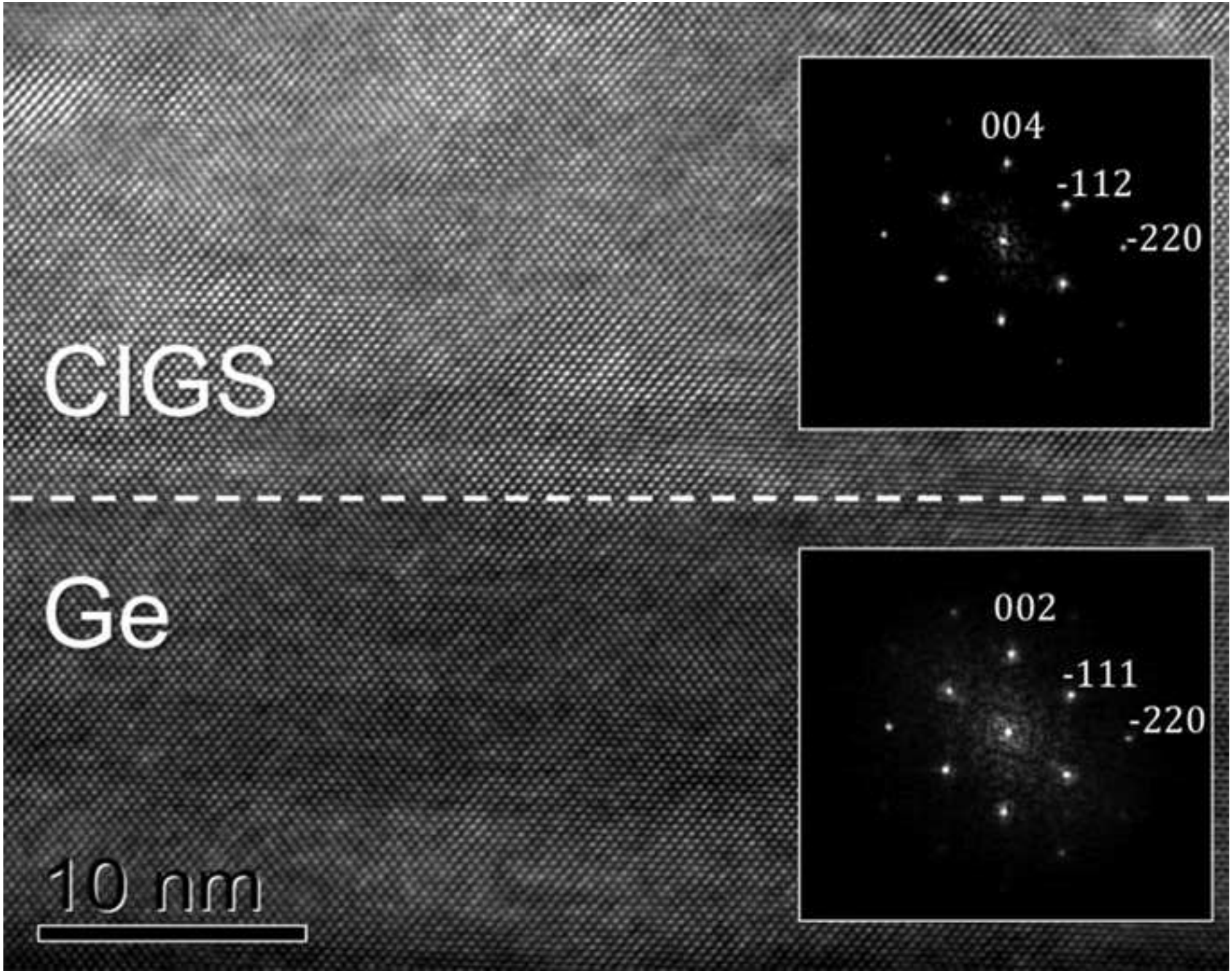

Figure 4

Click here to download high resolution image

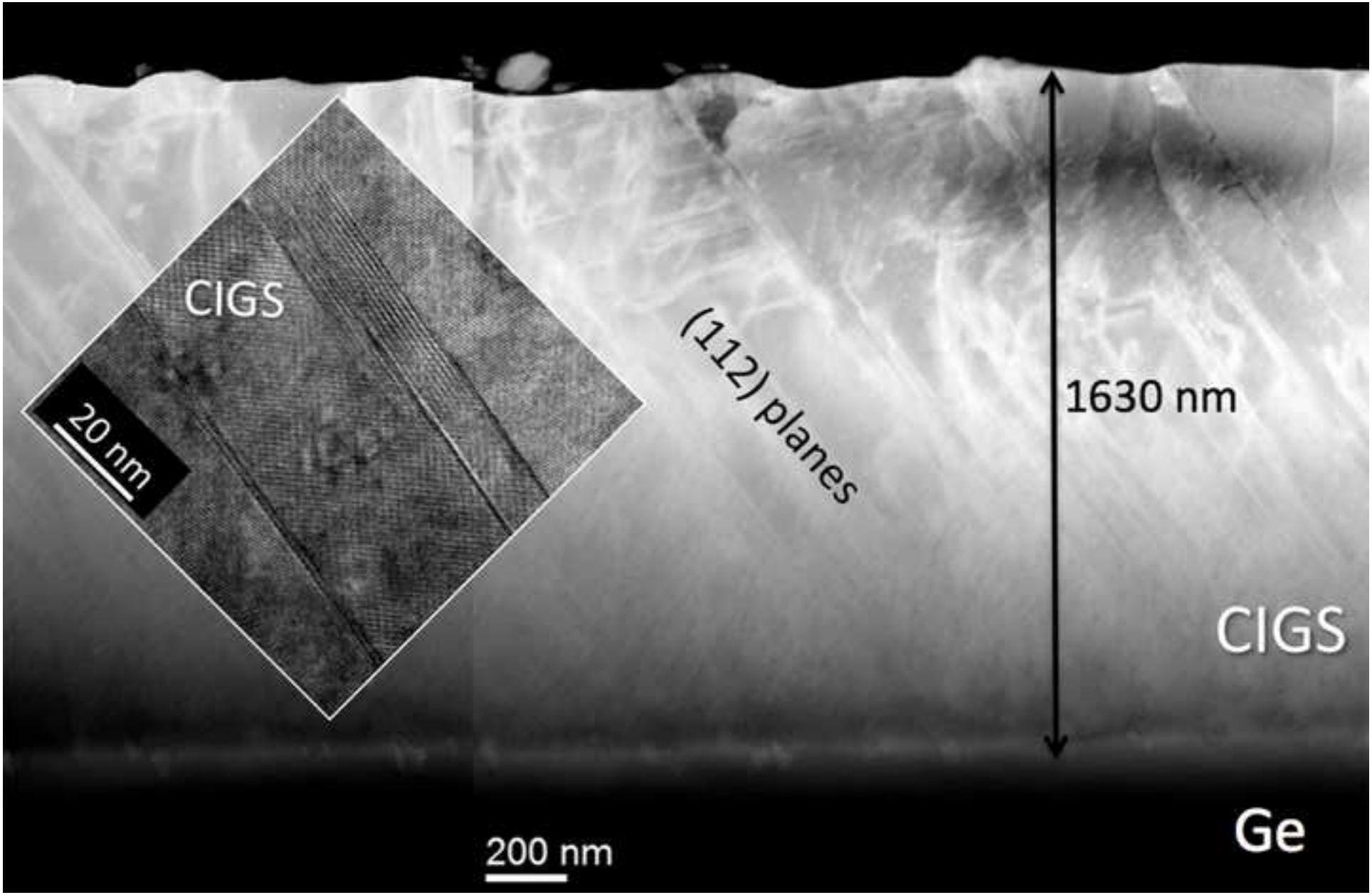

Figure 5

Click here to download high resolution image

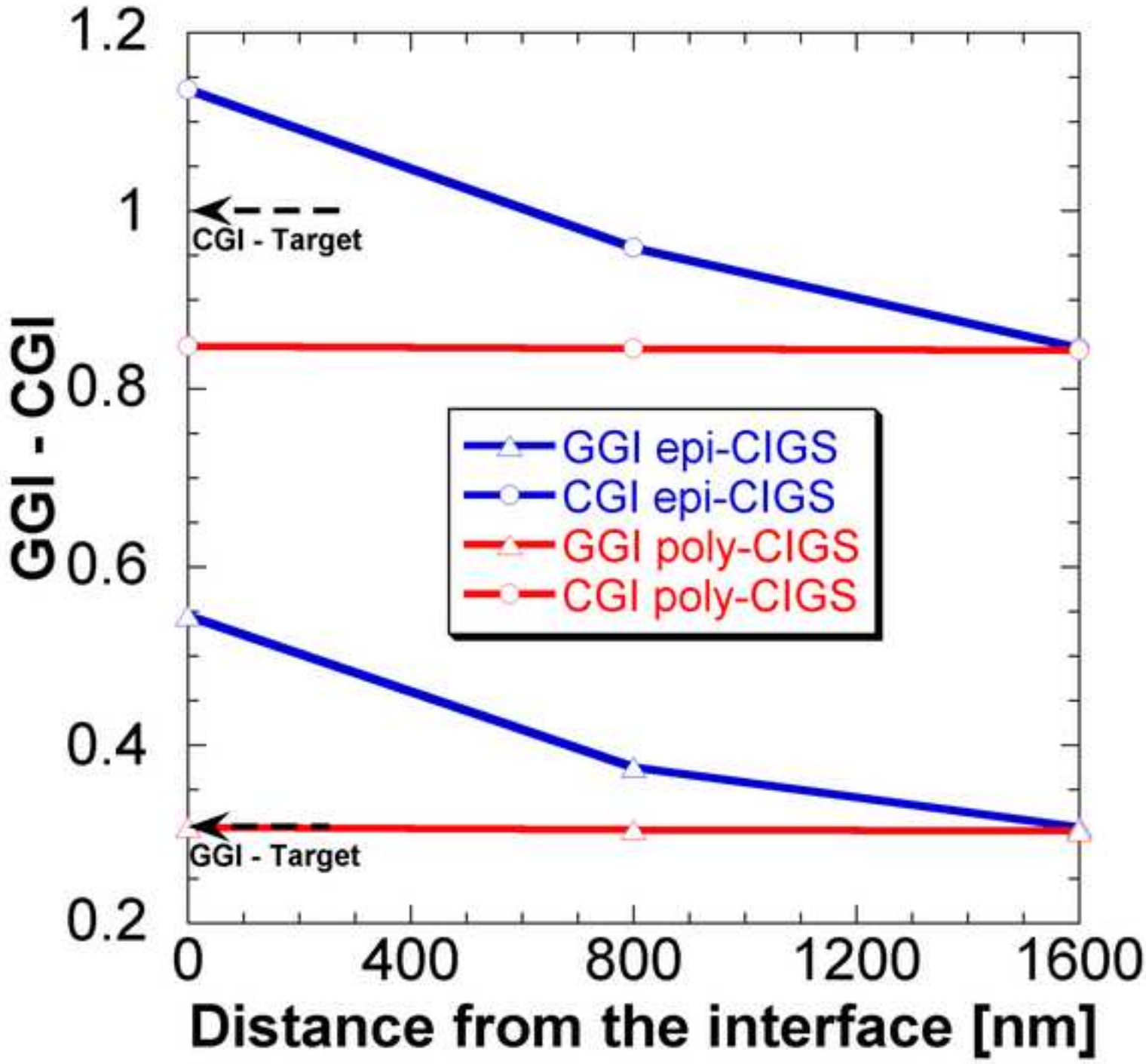

Figure 6

Click here to download high resolution image

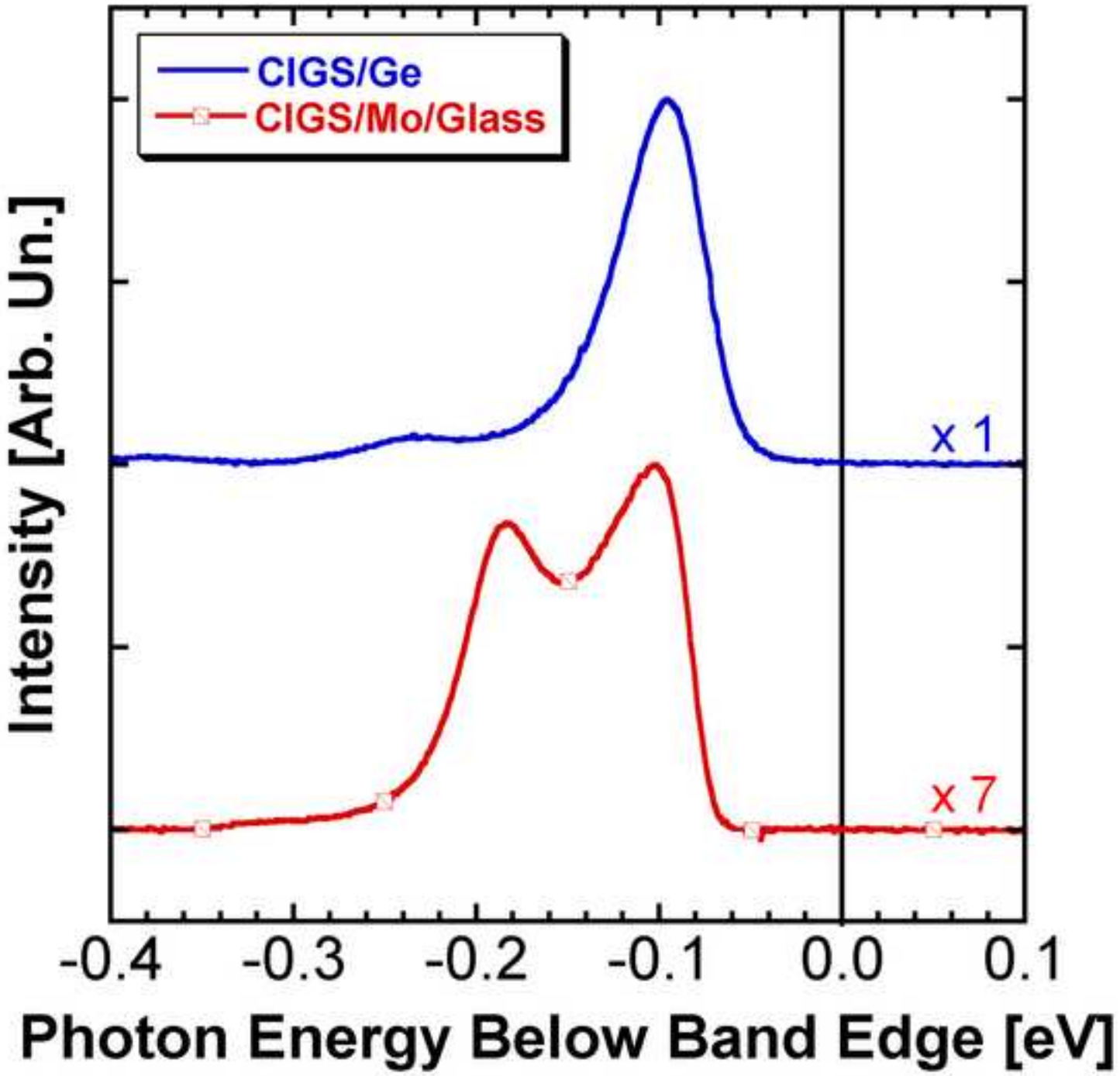

Figure 7
Click here to download high resolution image

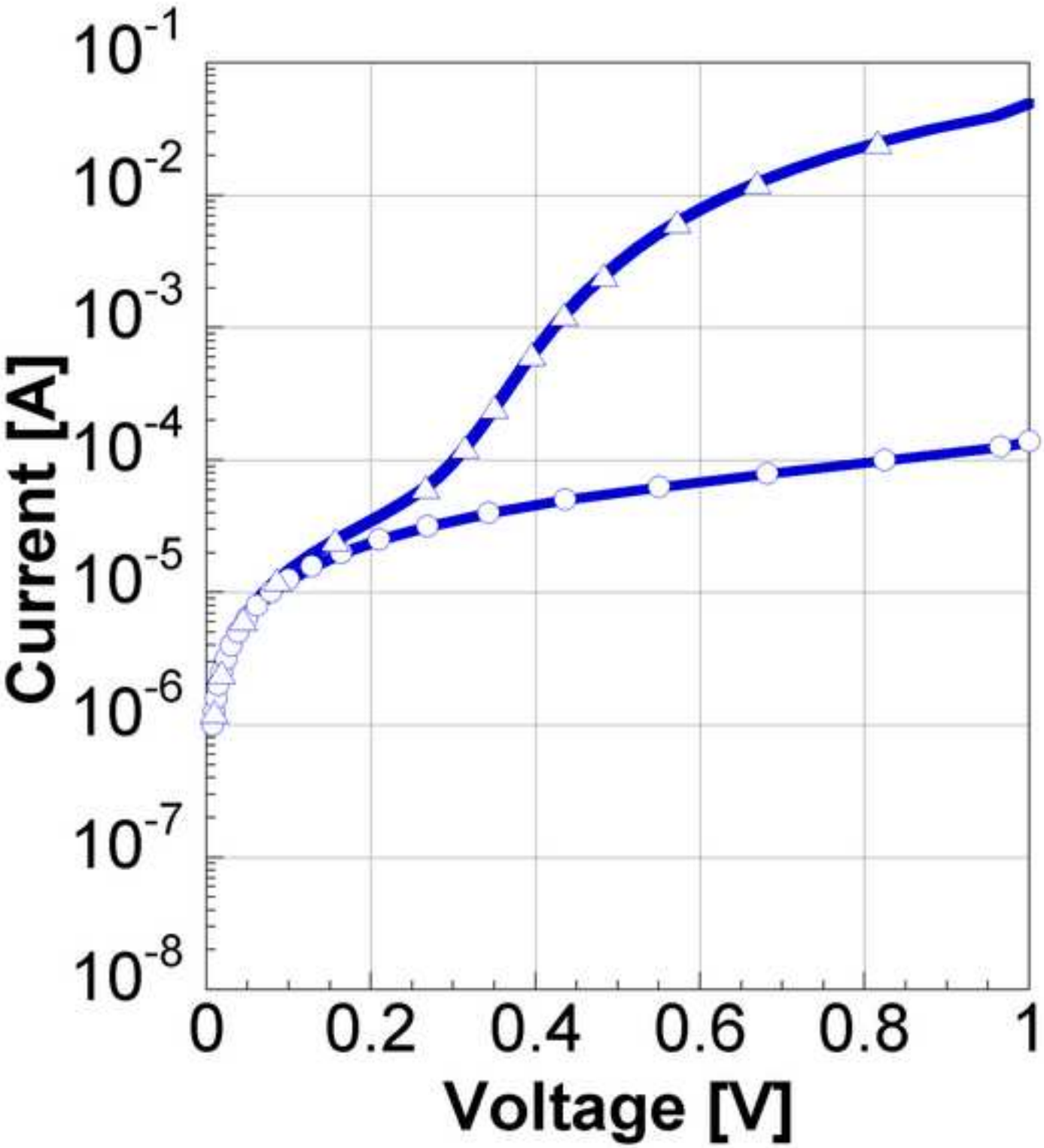

Figure 8

Click here to download high resolution image